Colloid Polym Sci 278:1139–1154 (2000)

ORIGINAL CONTRIBUTION

Chemical deposition and characterization of thin polypyrrole films on glass plates: role of organosilane treatment

C. Perruchot
M. M. Chehimi
M. Delamar
E. Cabet-Deliry
B. Miksa
S. Slomkowski
M. A. Khan
S. P. Armes

Received: 3 January 2000
Accepted: 19 May 2000

C. Perruchot · M. M. Chehimi (✉)
M. Delamar
ITODYS
Université Paris 7 – CNRS (UPRESA7086)
1 rue Guy de la Brosse, 75005 Paris, France
e-mail: chehimi@paris7.jussieu.fr
Fax: +33-1-44276814

E. Cabet-Deliry
Laboratoire d'Electrochimie Moléculaire
Université Paris 7, 2 place Jussieu
75005 Paris, France

B. Miksa · S. Slomkowski
Center of Molecular and Macromolecular Studies, Sienkiewicza 112
Lodz 90-363, Poland

M. A. Khan · S. P. Armes
School of Chemistry
Physics and Environmental Science
University of Sussex
Brighton BN1 9QJ, UK

Abstract Thin chloride-doped polypyrrole films (PPyCl) were deposited chemically onto untreated and silane-treated planar glass plates from aqueous solutions. The organosilanes used to treat the glass substrates were methyltriethoxysilane (C1), propyltrimethoxysilane (C3), octyltrimethoxysilane (C8) and aminopropyltriethoxysilane (APS). The decreasing order of hydrophobic character of silane-treated glass slides, as measured by water contact angle measurements, was glass–APS ≅ glass–C8 > glass–C3 > glass–C1 > glass. X-ray photoelectron spectroscopy was used to determine the surface chemical composition of the glass plates before and following coating with the silane coupling agents and/or the PPy thin layer, respectively. The attenuation in intensity of the glass Na_{1s} peak enabled the average thickness of the various organosilane overlayers to be estimated. Atomic force microscopy showed that the morphology of the organosilane overlayers was islandlike. The domains have a structure which depends upon the nature of the organosilane in question. Scanning electron microscope images showed that the morphology of the PPyCl thin films was homogeneous when coated onto glass–APS and glass–C8, but wrinkled at the surface of glass, glass–C1 and glass–C3 plates. Qualitative peel tests using 3M adhesive tape showed very good adhesion of PPyCl to the glass–APS substrate, whereas adhesion was fairly poor in the case of glass–PPy and PPy–alkylsilane–glass interfaces. The results of this multitechnique study suggest that hydrophobic interactions are important to obtain homogeneous and continuous thin PPy films, but Lewis acid–base interactions are the driving forces for strong and durable PPy–glass adhesion.

Key words Polypyrrole · Glass · Organosilanes · Wettability · Hydrophobic interactions

Introduction

Polypyrrole (PPy) is known to be insoluble, infusible and intractable after electrochemical (film) or chemical (powder) synthesis, which seriously limits its processability [1]. To overcome these poor mechanical properties, pyrrole polymerization must be carried out directly onto the substrate material of interest. Electrically conducting PPy films can be easily prepared electrochemically on conducting substrates, but only chemical synthesis can be employed with insulator substrates such as silica or glass. Many studies have reported the synthesis and characterization of PPy composites where an inorganic material has acted as a support for the in situ chemical synthesis of the conducting polymer or, alternatively, where the conducting polymer particles are dispersed in an insulating polymer matrix [2]. Maeda and Armes [3–4] reported the synthesis of PPy in the

presence of an ultrafine silica sol leading to unusual nanoscale hybrid PPy–silica particles with a raspberry morphology. Such particles possess a silica-rich surface as found by X-ray photoelectron spectroscopy (XPS) [5] and zeta-potential measurements [6]. These silica-rich nanocomposite particles could be surface-aminated using aminopropyltriethoxysilane (APS) [7]. Faverrole et al. [8] reported the preparation of conducting PPy-coated glass fibres where the glass fibre was pretreated with aminosilane and pyrrole-functionalized silane coupling agents before vapour-phase pyrrole polymerization. In the case of the pretreatment by pyrrole-functionalized silane, PPy adhesion to the glass fibre was found to be extremely strong. This is believed to be due to chemical bonding of PPy to glass via the pyrrole-functionalized silane coupling agent, which acts as a site for the polymerization initiation. Silica gel particles [9] and silica beads [10] have been modified by PPy to act as novel stationary reverse and anion-exchange phases in liquid chromatography. Improved selectivity of silica towards polyaromatic hydrocarbons was achieved after modification by PPy [10]. In the case of PPy coatings on octadecylsilane-treated silica beads (silica–C18–PPyCl), the capacity factors of several molecular probes were similar to those obtained with silica–C18, thus indicating that PPy did not contribute to the retention properties.

Silane coupling agents are a broad class of surface-modifying chemicals widely used as adhesion promoters in composite materials [11]. They are very effective in preparing grafted silica for selective interactions with analytes in liquid chromatography [12]. Surface modification of quartz by aminosilane led to the immobilization of dendrimers and polystyrene microspheres, both bearing surface aldehyde groups [13]. Organosilanes were also suggested as an alternative to the classical, but toxic, chromate rinse for corrosion control coatings on steel [14]. Of relevance to our ongoing research studies, Si/SiO_2 and glass surfaces were modified by C18 to act as templates for the selective deposition of conducting PPy and polyaniline [15]. Using patterned self-assembled monolayers of C18 as templates, it was possible to obtain patterned microstructures of conducting polymer coatings. Recently, we reported the effect of APS treatment of silica gel particles in the preparation of novel PPy–silica composite materials [16–17]. These composites were found to be conductive owing to a PPy-rich surface as a result of the in situ polymerization of pyrrole in the presence of APS-treated silica particles. The conductivity threshold was obtained for an initial APS concentration of 1% (v/v) although the weight percent of PPy did not exceed 12%. Moreover, the resulting conductive composite PPy–silica particles were found to be high-surface-area materials (160–180 m^2/g) compared to bulk PPy powder (15–25 m^2/g) [18].

In this work, we used glass-plate substrates as model planar surfaces for the chemical deposition of PPy in aqueous media. We wished to explore the effect of organosilane treatment of glass on the amount, morphology and adhesion of PPy coatings. Wettability by water, as determined by contact angle measurements, allowed us to quantify the hydrophobic character of untreated and silane-treated glass plates prior to pyrrole polymerization. XPS was used to monitor the change in the surface compositions of untreated and silane-treated glass plates before and after PPy deposition. The surface morphology of the untreated and silane-treated glass plates was observed by atomic force microscopy (AFM). In order to characterize the morphology of the PPy deposited onto untreated and silane-glass plates, PPy overlayers were imaged by scanning electron microscopy (SEM). Finally, adhesion of PPy to untreated and silane-treated glass plates was measured qualitatively by a simple peel test using 3M adhesive tape.

Experimental

Sample preparation

Chemicals

Pyrrole (Acros) was purified by passing it through a column of activated basic alumina prior to polymerization. Iron chloride (i.e. $FeCl_3{:}6H_2O$, Aldrich) was used as an oxidant/dopant species and was employed without further purification. Methyltriethoxysilane (C1, Aldrich, 99%), propyltrimethoxysilane (C3, Aldrich, 98%), octyltrimethoxysilane (C8, Aldrich, 96%) and APS (Aldrich, 98%) were used as received. Deionized water and ethanol (Prolabo, 95%) were used as solvents. Glass plates (Sientec, $2 \times 1 \times 0.1$ cm) were first washed for 30 min in KOH solution (5 mol l^{-1}) then rinsed with copious amounts of deionized water before silane treatment and PPy deposition.

Organosilane treatment of glass plates

Organosilane coupling agents (42.5 mmol l^{-1}) were first hydrolysed for 2 h in a stirred water/ethanol solution (10/90 v/v). Glass-plate substrates were then immersed for 6 h in the solution, allowing the condensation of the different coupling agents at the glass-plate surface. The organosilane-treated glass plates were then rinsed with copious amounts of deionized water in order to remove the excess of physically adsorbed coupling agents and were dried overnight in a desiccator prior to analysis.

Chemical deposition of PPy onto glass plates

Untreated and silane-treated glass plates were immersed vertically in a stirred aqueous solution (40 ml) containing iron chloride (36.0 mmol l^{-1}). Pyrrole (0.1 ml) was then injected via a syringe into the solution. The solution was stirred for 12 h to achieve complete chemical pyrrole polymerization. The PPy-coated glass plates were then carefully rinsed with deionized water to remove all excess oxidant/dopant species and were left to dry overnight in a desiccator prior to analysis.

X-ray photoelectron spectroscopy

The organosilane-treated and PPy-coated glass plates were mounted onto stubs using double-sided adhesive tape. XPS spectra were recorded using a VG Scientific ESCALAB MKI system operated in

the constant analyser energy mode. An Al Kα X-ray source was used at a power of 200 W (20 mA × 10 kV), and the pass energy was set at 20 eV. The pressure in the analysis chamber was about 5×10^{-8} mbar. Digital acquisition was achieved with a Cybernetix system and the data were collected with a personal computer. We used a nonlinear least-squares curve-fitting procedure to analyse the XPS spectra. The software allowed smoothing, linear and Shirley background removal, static charge referencing, peak fitting and quantification. The spectra were fitted with the sum of a series of components representing individual peaks characteristic of the chemical functional groups to unscramble the C_{1s} and N_{1s} peaks. Components of comparable binding energy positions were lumped together so that we kept the number of components (especially in the case of C_{1s}) as low as possible. The parameters associated with each peak were binding energy peak centre, peak height, full width at half maximum (FWHM) and the Gaussian-to-Lorentzian ratio. No tailing function was considered in the peak-fitting procedure. Peak fitting was performed manually in a first stage then optimized by the curve-fitting software. We kept the FWHM of the various components of a given spectrum as close as possible with a difference up to ±0.1 eV. The quality of the curve fit was obtained by the determination of χ^2, the sum of the squares of the difference between the experimental spectrum and the theoretical fitted envelope at each point (0.1 eV) over the peak region of interest. In performing the curve fitting we tried to reach the "best fit" which is consistent with chemical meaning. Charge referencing was determined by setting the main C_{1s} component, i.e. C-C/C-H, at 285.0 eV in the case of organosilane-treated glass plates or the main N_{1s} component due to the N-H group at 399.7 eV in the case of PPy-coated plates. The surface composition (in atomic percent) of the various samples was determined by considering the integrated peak areas of C_{1s}, N_{1s}, O_{1s}, Si_{2p}, Cl_{2p}, Na_{1s} and Fe_{2p} and using their respective experimental sensitivity factors. The experimental sensitivity factors were C_{1s}(1), N_{1s}(1.6), O_{1s}(3.1), Si_{2p}(1.2), Cl_{2p}(2.8), Na_{1s}(11.5) and $Fe_{2p3/2}$(7.8).

The fractional concentration of a particular element A (%A) was computed using

$$\%A = \frac{(I_A/s_A)}{\sum(I_n/s_n)} \times 100\% \quad , \qquad (1)$$

where I_n and s_n are the integrated peak areas and the sensitivity factors, respectively.

Scanning electron microscopy

SEM images of PPy coated onto untreated and silane-treated glass plates were obtained using a Leica Stereoscan 420 instrument operating at 30 kV with a probe current of 10 pA. The samples were mounted onto a doubled-sided adhesive carbon disk and sputter-coated with a thin layer of gold to prevent sample charging during analysis.

Contact angle measurements

Contact angle measurements were performed on untreated and organosilane-treated glass plates with a Rhame Hart contact angle goniometer equipped with an environmental chamber which allowed the temperature to be constant over the time scale of the measurements. Deionized water (2 μl) was used as a probe liquid. The contact angles obtained were average values of at least six different drops of water to ensure good repeatability of the results. For all plates under investigation, the standard deviation of the contact angle was less than ±2°.

Atomic force microscopy

Untreated and silane-treated glass plates were imaged by a Nanoscope III Digital Instrument in the tapping mode using a Si_3N_4 tip cantiliver. The cantiliver oscillation frequency was set at 300 kHz. The tips of the cantiliver were characterized by the radius of their curvature, which was 7 ± 2 nm. No computer filtering procedure was used to treat the images. Tapping mode images were recorded with 256 pixels per line with a scan rate of 2.0 Hz. Surface roughness was determined on the same scale (1 μm) for each sample.

Results and discussion

Wettability of the silane-treated glass plates

The wettability of untreated and silane-treated glass plates was determined by contact angle measurements using a sessile drop method. In these experiments, deionized water was used as the reference liquid. The results of contact angle measurements for untreated and silane-treated glass plates are shown in Fig. 1. The untreated glass plate exhibits the lowest contact angle (about 35°). This hydrophilic character is due to the presence of silanol groups (SiOH) at the outermost glass surface which interact favourably with water via hydrogen bonding. However, surface modification of the glass plates with alkylsilane led to a significant increase in the contact angles since alkyl groups are hydrophobic. It is worth noting that increasing the length of the alkyl chain resulted in a lower wettability, thus showing that the alkyl groups constitute the outermost layer of the modified glass surface. For the glass–APS plate, in spite of the intermediate length of the pendant chain and the basic amino end groups, hydrophobic character similar to that of glass–C8 was exhibited. This shows that both the nature and the length of the pendant functional group affect wettability.

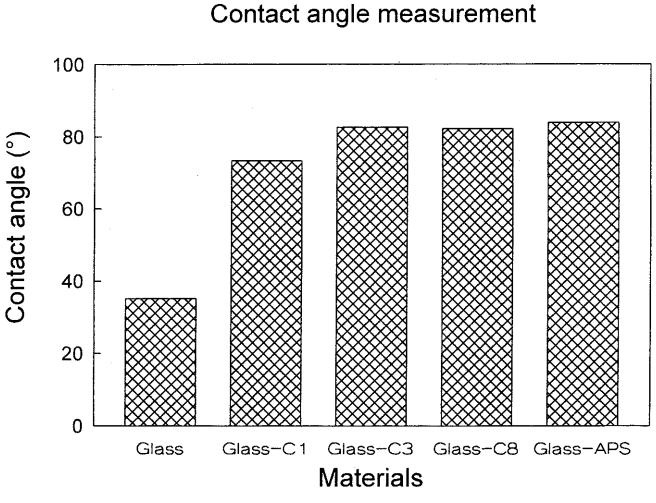

Fig. 1 Water contact angles at the surface of untreated and silane-treated glass plates. *C1*: methyltriethoxysilane; *C3*: propyltrimethoxysilane; *C8*: octyltrimethoxysilane; *APS*: aminopropyltriethoxysilane

XPS characterization of organosilane treatment and PPy coating of glass

XPS was used to characterize the chemical structure and composition of the untreated and silane-treated glass plate surfaces before and after PPy deposition. Since we used planar surfaces, angle-dependent XPS (ADXPS) measurements were performed in order to obtain a nondestructive depth profiling of the untreated and silane-treated glass plates (analysed at two different angles, 90° and 45° relative to the surface). In the case of PPy deposition onto untreated or silane-treated glass plates, XPS analysis was performed at 90°.

Survey spectra

XPS survey spectra of untreated glass, glass–C8, glass–PPy and glass–C8–PPy are shown in Fig. 2. For untreated and silane-treated glass plates (Fig. 2a, b), typical Si_{2p}, Si_{2s}, O_{1s}, O_{KLL}, Na_{KLL} and Na_{1s} signals from the glass substrates were detected. For alkylsilane-treated glass plates, an additional carbon signal (C_{1s}) from the alkyl chain was also detected. Similar XPS survey spectra were obtained for glass–C1 and glass–C3 plates. In the case of glass–APS (not shown), an additional low-intensity N_{1s} peak due to the amino group from APS was detected. Increasing the alkyl chain length of the organosilane leads to an increase in the relative intensity of the C_{1s} peak (Fig. 2b), which is in contrast to a dramatic attenuation of the Na_{1s} signal from the glass substrate (Fig. 2a). It is also noted that in the case of glass–C8, the Na_{KLL} line from glass is much less attenuated than the Na_{1s} because the Auger electron has a much higher kinetic energy (990 eV) and thus a higher analysis depth than that of the photoelectron (Na_{1s} kinetic energy = 414 eV).

In the case of glass–PPy (Fig. 2c) and glass–C8–PPy (Fig. 2d), intense C_{1s} and N_{1s} peaks due to the PPy overlayer were detected. Additional iron (Fe_{2p} and Auger Fe_{LMM}) and chloride peaks (Cl_{2p}) due to the oxidant/dopant species were also observed. Simultaneously, a strong depletion of the silicon Si_{2p} and Si_{2s} photopeaks due to the additional silane and PPy overlayers is very noticeable. Whilst the Na_{1s} and Na_{KLL} lines appear slightly attenuated for glass–PPy (Fig. 2c) in comparison to glass (Fig. 2a), they are no longer detected on the survey spectrum of glass–C8–PPy (Fig. 2d).

Further confirmation of the attenuation of the substrates by PPy is the dramatic change in the intensity of the spectral background observed in Fig. 2c and d due to inelastically scattered electrons from glass.

C_{1s} spectra

High-resolution C_{1s} spectra of glass–APS, glass–PPy and glass–APS–PPy are shown in Fig. 3.

The C_{1s} signal from untreated glass plate (not shown) was fitted with two components centred at 285.0 and 288.8 eV, corresponding to carbon contamination (*C*-C/*C*-H) and carboxylic and/or ester functional groups (-*C*OOH or -*C*OOR).

For alkylsilane-treated glass plates (not shown), peak fitting of the carbon signal was achieved with one peak for glass–C1, centred at 284.1 eV corresponding to *C*-Si bonds, whereas for glass–C3 and glass–C8 plates, the C_{1s} signal was fitted with two components centred at 284.0 and 285.0 eV corresponding to *C*-Si and *C*-C/*C*-H bonds, respectively [11]. For the glass–APS plate (Fig. 3a), the C_{1s} signal was peak-fitted with three components centred at 284.1, 285.0 and 286.0 eV due to Si-*C*-C, C-*C*-C and C-*C*-N bonds, respectively [11, 16]. It should be noted that the high-binding-energy component (due to -*C*OOR) of the untreated glass disappeared after silane treatment, showing that the alkyl or aminosilane species at least partially removed the contaminant species from the glass surface.

Peak fittings and peak area ratios corresponding to the different carbon species from the various silane-treated glass plates are reported in Table 1. It is noteworthy that the peak area ratios are in good agreement with theoretical formulae of the alkylsilane and aminosilane coupling agents, although for the latter there is evidence for some adventitious hydrocarbon contamination contributing to the C_{1s} component centred at 285 eV.

In the case of the glass–PPy (Fig. 3b) and glass–APS–PPy (Fig. 3c) plates, there is a dramatic change in the shape of the C_{1s} signal as a result of PPy deposition. For PPy deposition onto silane-treated glass plates, both the silane coupling agent and PPy overlayers contribute to the carbon signal. However, for all substrates, the C_{1s} signal has a shape that is frequently reported for bulk PPy. This complex signal is fitted with five components attributable to the β carbon from PPy (285.0 eV), the α carbon (285.7 eV) and higher-binding-energy features at 287.4 and 289.0 eV which correspond to "disorder-type" carbon and terminal N-*C*=O or *C*OOH groups. It should be pointed out that these two latter components are more predominant than in the case of bulk PPy film or powder synthesis in aqueous media. This clearly demonstrates that the PPy chains have many oxidized end groups, perhaps due to the low concentration of pyrrole used for the polymerization or to the direct interaction of surface hydroxyl groups from the glass plates with the polymer chain. The high-binding-energy component centred at 291.5 eV is attributed to a $\pi \rightarrow \pi^*$ shake-up transition due to the conjugated PPy chain.

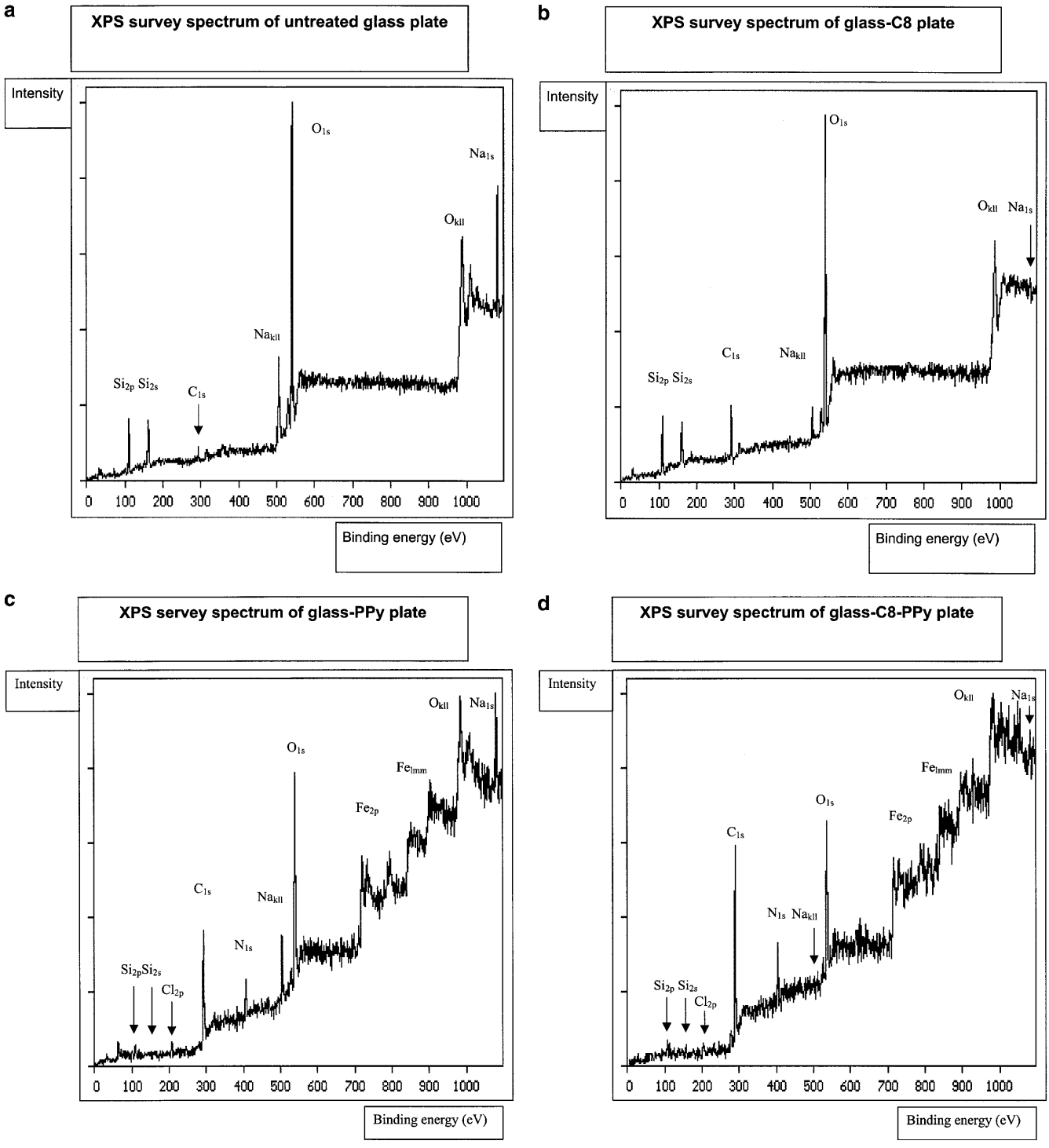

Fig. 2 X-ray photoelectron spectroscopy survey spectra of **a** untreated glass, **b** glass–C8, **c** glass–polypyrrole (*PPy*) and **d** glass–C8–PPy

The relative peak intensity ratios corresponding to the different components of the C_{1s} regions from PPy deposited onto untreated and silane-treated glass plates are reported in Table 2.

Although the shape of the C_{1s} peak for PPy-coated glass plates is comparable to that of PPy bulk powder, there is a substantial effect of the silane coupling agent on the weight of the C_{1s} C-C/C-H component at 285.0 eV. Indeed, the relative area of this component increases with the number of carbon atoms in the corresponding organosilane.

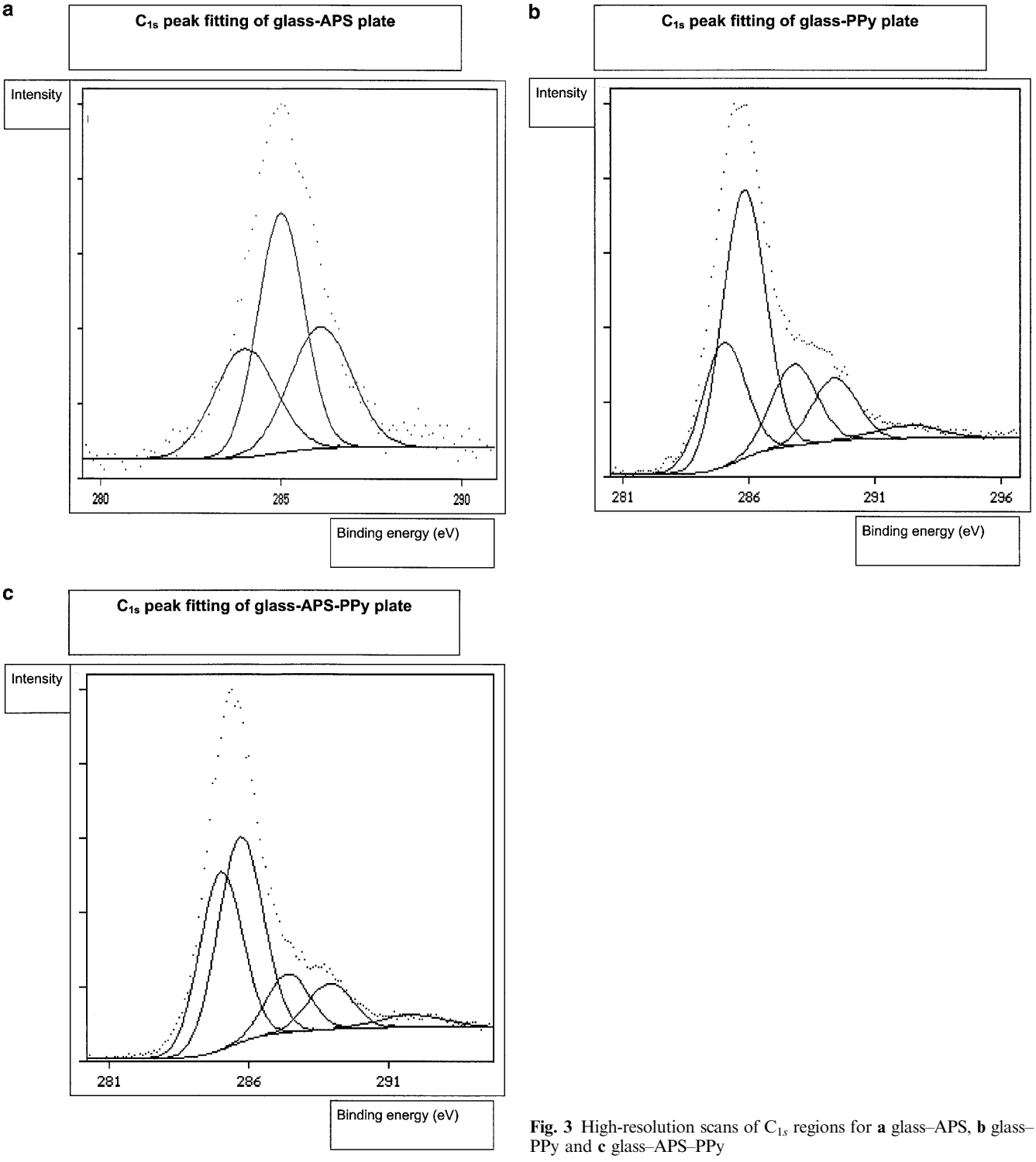

Fig. 3 High-resolution scans of C_{1s} regions for **a** glass–APS, **b** glass–PPy and **c** glass–APS–PPy

N_{1s} spectra

Peak-fitted high-resolution N_{1s} spectra of glass–APS, glass–PPy and glass–APS–PPy are displayed in Fig. 4.

For the glass–APS substrate (Fig. 4a), nitrogen is a unique elemental marker for the APS overlayer. The N_{1s} signal was peak-fitted with two components centred at 399.6 and 401.8 eV, attributed to free amine groups and

Table 1 Carbon peak fitting and relative peak area ratios for silane-treated glass plates determined by X-ray photoelectron spectroscopy (*XPS*). *C1*: methyltriethoxysilane; *C3*: propyltrimethoxysilane; *C8*: octyltrimethoxysilane; *APS*: aminopropyltriethoxysilane

Substrate	Glass–C1	Glass–C3		Glass–C8		Glass–APS		
Peak fitting (eV)	284.0	284.0	285.0	283.8	285.0	284.1	285.0	286.0
Peak area ratio (%)								
Experimental	100	33.2	66.8	14.0	86.0	27.4	41.5	31.1
Theoretical	100	33.3	66.7	12.5	87.5	33.3	33.3	33.3

Table 2 Relative peak intensity ratios (%) of the peak fitted C_{1s} signal of thin polypyrrole (*PPy*) films deposited onto untreated and silane-treated glass plates as determined by XPS

C_{1s} peak fitting (eV) Sample	285.0	285.7	287.4	289.0	291.5
Glass–PPy	22.1	47.8	15.1	11.7	3.3
Glass–C1–PPy	36.1	37.0	13.3	9.3	4.3
Glass–C3–PPy	45.8	32.2	12.7	7.7	1.6
Glass–C8–PPy	53.1	28.7	10.2	6.2	1.8
Glass–APS–PPy	34.2	41.7	11.3	9.2	3.6

to an ammonium or -SiOH…H_2N- hydrogen bond, respectively. This result is in good agreement with previously published results concerning APS modifications of glass plates [19], quartz plates [20] and silica gel particles [16].

In the case of PPy deposited onto untreated (Fig. 4b) and alkylsilane-treated glass plates (spectra not shown), the nitrogen signal is similar to that of the N_{1s} structure usually reported in the literature for bulk PPy film or powder. The N_{1s} signal was peak-fitted with four components due to the imine defects (397.8 eV), free N-H from pyrrole repeat units (399.7 eV), C-N^+ (400.8 eV) and C=N^+ (402.3 eV) [21, 22]. However, the contribution of the positively charged nitrogen atoms is higher for the glass–PPy than the glass–C3–PPy and the glass–C8–PPy interfaces.

For PPy deposited onto the APS-treated glass plate (Fig. 4c), the N_{1s} signal was peak-fitted with four components as in the case of glass–PPy and glass–alkylsilane–PPy; however, the contribution of APS to the N_{1s} peak shape should be noted since the most intense component is now centred at 401.1 eV and no longer at 399.7 eV, as in the case of bulk powder PPy [21], glass–PPy and glass–alkylsilane–PPy. This significant change in the shape of the N_{1s} signal can be explained as follows. APS is a Brönsted base and can be protonated or interact via hydrogen bonding. At the APS/PPy interface, APS may interact via hydrogen bonding with PPy acting as a Lewis acid [23]. In this case, the free amine from APS undergoes a positive chemical shift due to the charge transfer towards the acidic PPy. This chemical shift can be as high as 1–2 eV as in the case of the Brönsted base pyridine adsorbed onto zeolites [24] and polymers [25–26]. As mentioned earlier, the high-binding-energy component of the N_{1s} signal from glass–APS (Fig. 4a) is due to protonation or hydrogen bonding of the APS with the hydroxide groups at the glass surface. This situation is likely to remain the same so that both former types of nitrogen atoms at the glass–APS surface are now either protonated or interact via hydrogen bonds with both glass and PPy.

Surface composition

The surface composition (calculated using Eq. 1) of untreated and silane-treated glass plates at two different angles as determined by XPS is reported in Table 3.

Since the untreated glass plate exhibits a low degree of carbon contamination, surface modification by the silane coupling agent was monitored via the attenuation of the Na_{1s} peak from the glass substrate. For alkylsilane treatment, the atomic percent of carbon was found to increase with the increasing number of carbon atoms per organosilane coupling agent. In the case of the APS-treated glass plate, the nitrogen detected is solely due to APS since nitrogen is a unique elemental marker for the grafted APS coupling agent. The amount of carbon at the surface is similar to that for glass–C3 since APS and C3 have, in fact, quite similar lengths of the functional chains. The sodium content decreases and its relative surface composition is similar to that detected for C3 silane. It is worth pointing out that an increase in the carbon content for all the silane-treated glass plates correlates fairly well with increasing hydrophobic character as determined by contact angle measurements.

ADXPS shows a higher C_{1s} peak intensity at 45°, especially in the case of glass–C8 and glass–APS. This clearly demonstrates the presence of a thin overlayer of the silane-coupling agent at the glass surface. Using ADXPS, we estimated the thickness of the silane overlayers using the Beer–Lambert equation applied for the Na_{1s} core hole (unique elemental marker for glass substrate):

$$I_{\mathrm{Na}_{1s}} = I^{\infty}_{\mathrm{Na}_{1s}} * \exp\left(\frac{-d}{\lambda_{\mathrm{Na}_{1s}} \sin\vartheta}\right) , \qquad (2)$$

where $I_{\mathrm{Na}_{1s}}$ is the intensity of the Na_{1s} signal from the silane-treated glass plate, $I^{\infty}_{\mathrm{Na}_{1s}}$ is the Na_{1s} peak intensity for an infinitely thick glass substrate (in this case untreated glass substrate), $\lambda_{\mathrm{Na}_{1s}}$ is the Na_{1s} electron

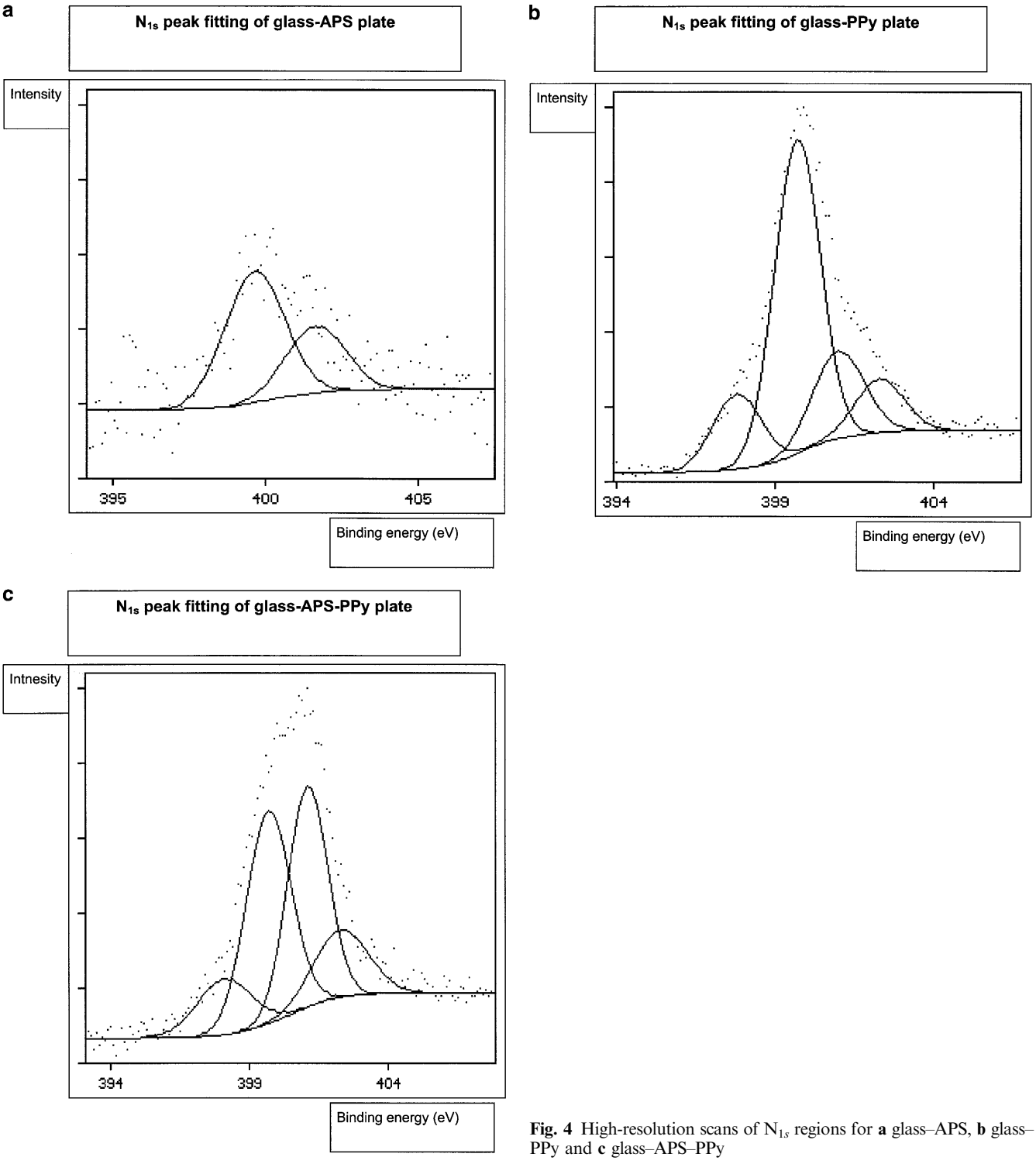

Fig. 4 High-resolution scans of N_{1s} regions for **a** glass–APS, **b** glass–PPy and **c** glass–APS–PPy

mean free path in the organosilane overlayer and θ is the take-off angle relative to the surface.

ADXPS enables the overlayer thickness to be determined using the following equation:

$$d = \frac{\lambda_{\mathrm{Na}_{1s}}}{\left[\sin^{-1}(\vartheta 2) - \sin^{-1}(\vartheta 2)\right]} \ln\left(\frac{I_{\vartheta 1}}{I_{\vartheta 2}}\right) , \quad (3)$$

Table 3 Surface composition (atom %) of untreated and silane-treated glass plates as determined by XPS

Sample	Angle (°)	C	N	O	Si	Na
Glass	90	5.62	–	62.56	25.46	6.36
	45	9.55	–	59.30	25.33	5.83
Glass–C1	90	5.29	–	65.76	26.84	2.11
	45	5.83	–	65.16	26.98	2.02
Glass–C3	90	8.61	–	62.61	27.02	1.75
	45	10.72	–	60.62	26.62	2.04
Glass–C8	90	22.95	–	51.70	24.31	1.04
	45	28.22	–	47.36	23.45	0.96
Glass–APS	90	9.12	1.54	62.06	25.41	1.88
	45	13.57	1.68	57.44	25.49	1.82

where I_θ is the Na_{1s} peak intensity at a given take-off angle.

$\lambda_{Na_{1s}}$ can be calculated using the equation of Seah and Dench [27]:

$$\lambda = 0.11E_k^{1/2} + 49E_k^{-2}\,\mathrm{mg/m^2} \quad , \tag{4}$$

where E_k is the kinetic energy (eV) of a particular electron crossing the overlayer.

For a Na_{1s} photoelectron, E_k is computed by

$$E_k = h\nu - E_b \quad , \tag{5}$$

where $h\nu$ is the X-ray energy (1486.6 eV) and E_b the Na_{1s} binding energy (about 1072 eV). Therefore E_k = 414.6 eV and, neglecting the second term in Eq. (4), λ = 2.24 mg/m^2.

The conversion of milligrams per square metre to nanometres is obtained from the expression

$$\lambda(\mathrm{nm}) = \lambda(\mathrm{mg/m^2})/\rho \quad , \tag{6}$$

where ρ is the overlayer density in grams per cubic centimetre. For organosilanes, we assumed ρ = 1.5 g/cm^3 and thus $\lambda_{Na_{1s}}$ = 1.49 nm.

The estimated thickness for organosilanes grafted at the surface of glass is reported in Table 4.

The surface compositions (calculated using Eq. 1) of glass–PPy and glass–silane–PPy plates as determined by XPS are reported in Table 5. One can note the dramatic change in the carbon and nitrogen contents due to the deposition of PPy overlayers. A slight increase in the carbon content is also noted as a result of increasing chain length in the alkylsilanes. The C/N atomic ratio is slightly above the theoretical value of 4 because of the contribution of the silane coupling agents. Moreover, the O/Si atomic ratio is much higher than the theoretical value of 2. This is mainly due to the simultaneous attenuation of Si_{2p} from the glass plate and to the surface oxidation of PPy as judged by the C_{1s} signal shown in Fig. 3b. This peak exhibits a shoulder at high binding energy as previously described. Since glass is the only sodium-containing material, the PPy overlayer leads to a strong attenuation of the Na_{1s} peak from the inorganic substrate. This attenuation is exacerbated when PPy is coated onto silane-treated glass plates.

Table 4 Organosilane overlayer thickness on glass substrates as determined by angle-dependent XPS

Sample	Thickness (nm)
Glass–C1	3.9
Glass–C3	4.6
Glass–C8	5.7
Glass–APS	4.1

The doping level (Table 6) is calculated by determining the Cl/N atomic ratio and peak area intensity ratio from the nitrogen peak fitting ($I_{N^+}/I_{N_{tot}}$). For PPy deposited onto the untreated glass plate, the doping level (23.5%) is similar to that usually reported for PPy film or powder, i.e. 25–30% [21, 28]; however, in the case of PPy deposited onto silane-treated glass plates, a slight decrease in the doping level is observed (17.4–20.5%). It is also noted that for glass and silanized glass substrates, the doping levels calculated by both approaches lead to similar values except for the APS–treated glass. In the latter case, a very high N^+/N_{tot} ratio is obtained because of the contribution of the APS moiety.

Surprisingly, the iron content of the PPy-coated substrates is very high. We have already attributed iron to $FeCl_2$ and/or $FeCl_4^-$ (codopant) species [28]; however, in the present study these iron-containing species cannot account for the much lower Cl content compared to that of Fe.

AFM characterization of untreated and silane-treated glass substrates

AFM was used to investigate the surface morphology of the untreated and silane-treated glass plates. AFM

Table 5 Surface composition (atom %) of glass–PPy and glass–silane–PPy plates as determined by XPS

Sample	C	N	O	Si	Na	C1	Fe
Glass–PPy	45.18	9.29	27.19	2.00	2.44	2.18	11.72
Glass–C1–PPy	50.18	10.88	21.64	2.53	0.64	2.27	11.85
Glass–C3–PPy	52.69	10.41	22.21	3.72	0.46	1.82	8.68
Glass–C8–PPy	59.50	9.89	20.28	3.29	Trace	1.72	5.33
Glass–APS–PPy	50.30	9.25	23.25	2.58	0.54	1.80	12.28

Table 6 Doping level of the PPy overlayer on untreated and silane-treated glass plates as determined by XPS

Doping level (%) Sample	C1/N	N^+/N_{tot}
Glass–PPy	23.5	28.0
Glass–C1–PPy	20.8	26.3
Glass–C3–PPy	17.5	24.5
Glass–C8–PPy	17.4	20.8
Glass–APS–PPy	19.5	49.1

images of glass–Cl, glass–C3, glass–C8 and glass–APS are displayed in Fig. 5.

The average roughness of the various untreated and silane-treated glass plates, as determined by AFM, is reported in Table 7.

The morphology of the reference untreated glass substrate (AFM image not shown) is homogeneous and exhibits the lowest roughness. Alkylsilane treatment led to an ''islandlike'' surface morphological structure of

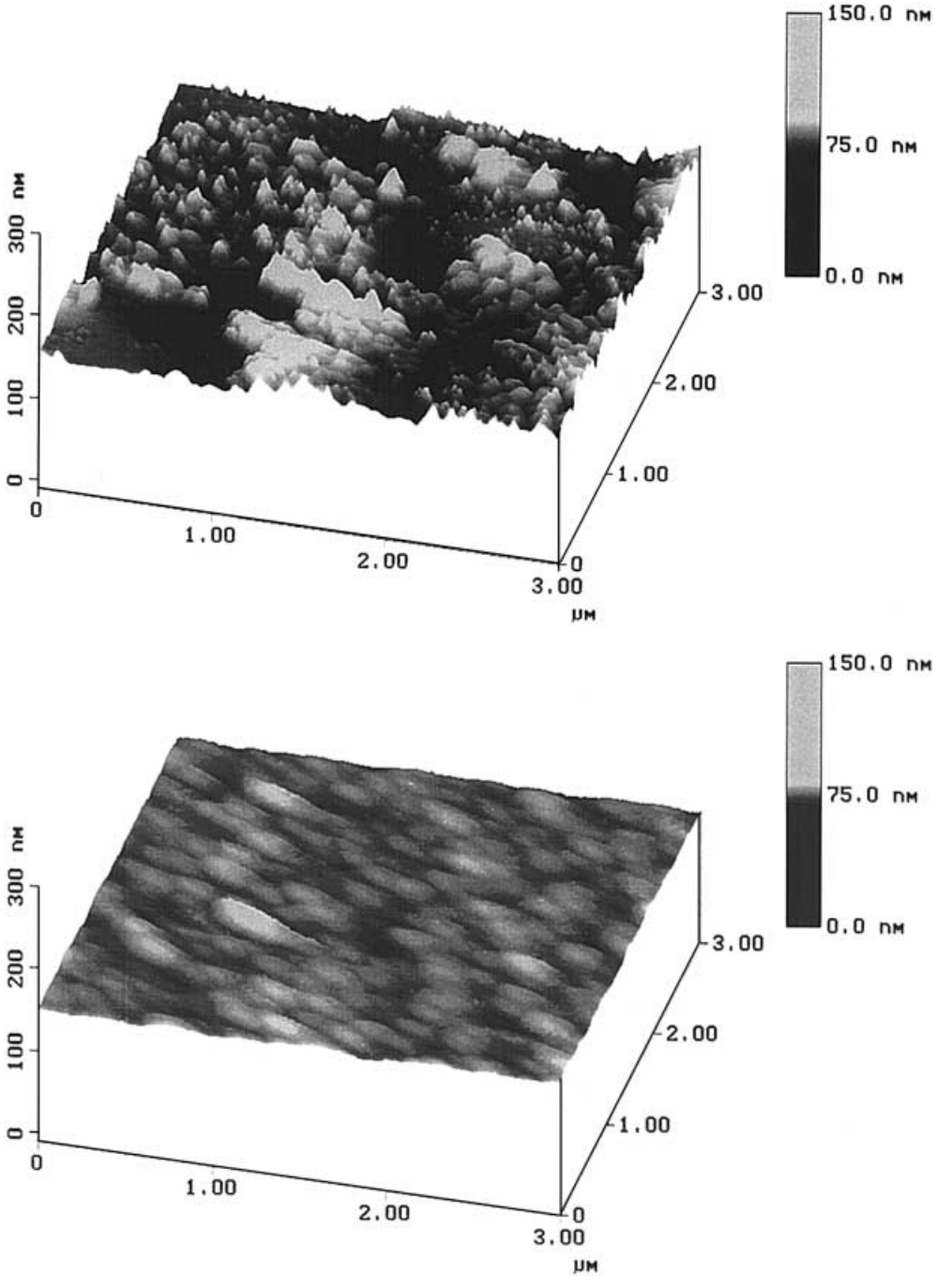

Fig. 5 Atomic force microscope images of **a** glass–C1, **b** glass–C3, **c** glass–C8 and **d** glass–APS

Fig. 5. (Contd.)

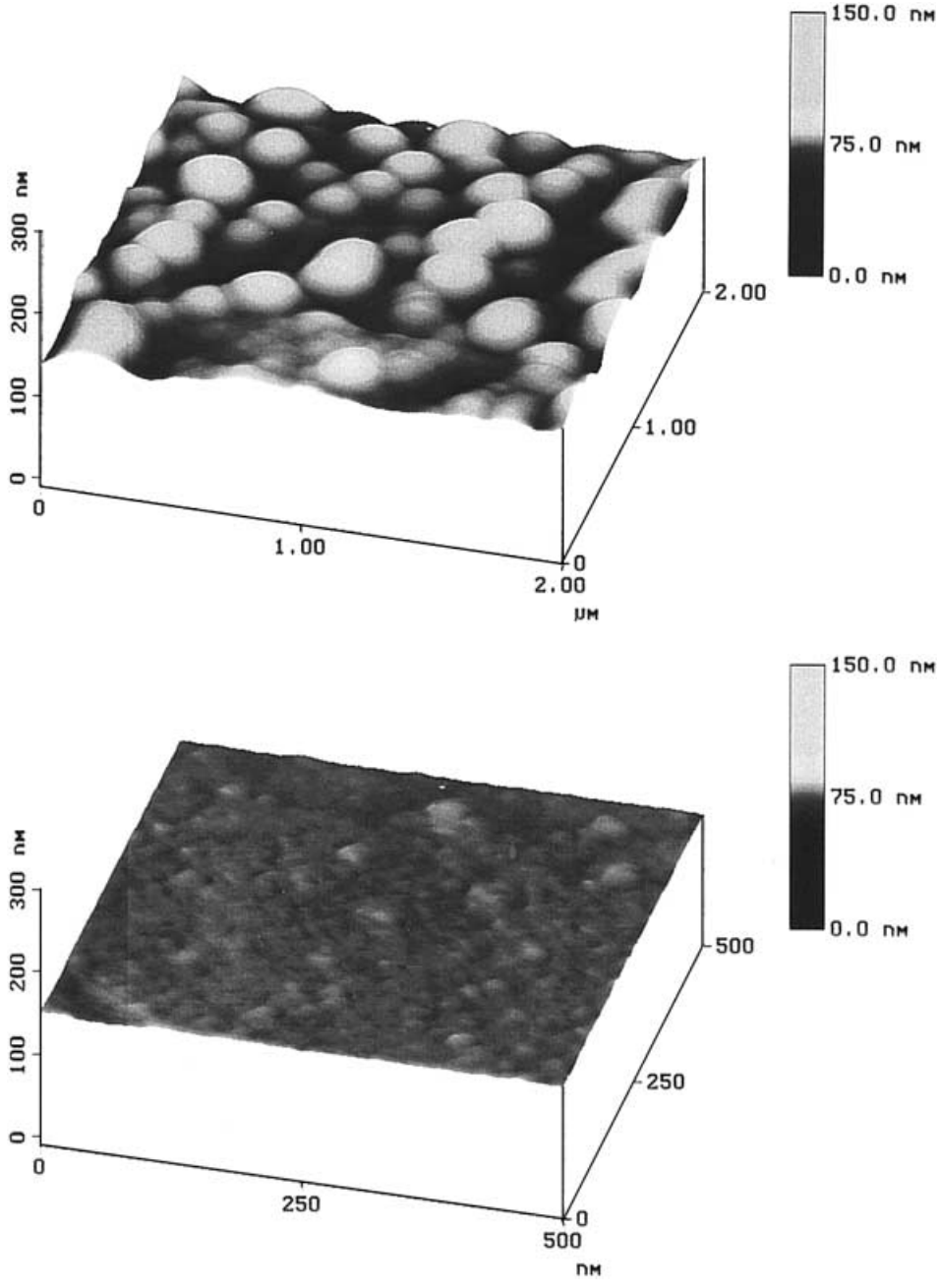

which the density and diameter increased with the size of the alkyl chain. Glass–Cl (Fig. 5a) appears to be a very rough substrate and exhibits a nonuniform and noncontinuous silane overlayer. These silane patches are sharp and have a wide distribution of height and diameter ranging from 10 to 100 nm. It should be noted that the methylsilane dots are aligned in a preferential direction of about 150° relative to the tip scanning. This alignment may be induced by the glass scratches, if there are any. The glass–C3 substrate (Fig. 5b) shows a much more homogeneous and continuous alkylsilane overlayer, leading to a much smoother surface than that of glass–C1. Glass–C3 exhibits domains of 100 ± 20-nm diameter which are randomly distributed at the glass surface. The glass–C8 substrate (Fig. 5c), however, displays a surface morphology which differs markedly from those of glass, glass–C1, and glass–C3. Indeed, C8 grows as microspheres of 200 ± 50-nm diameter at the glass surface. Moreover, these microspheres are closely packed, perhaps for surface-energy-minimization considerations. C8 deposition is constituted of domains of three adjacent microspheres,

the centres of which form an equilateral triangle. The surface roughness of glass–C8 is much higher than that of glass–C3 and compares more with that of glass–C1; however, as shown in Fig. 5a–c, the width and distribution of the silane domains are very different, depending on the length of the alkyl chain. The glass–APS substrate (Fig. 5d), on the other hand, exhibits a well-coated, homogeneous and continuous silane overlayer. The surface morphology is made of nanospheres of 15 ± 5-nm diameter. Moreover, the surface roughness is the lowest and is of the same order of magnitude as that of the untreated glass substrate. These nanospheres observed at the glass–APS surface seem to be as randomly distributed as the ''needles'' observed at the surface of untreated glass. However, the height of the glass–APS is higher than that of glass, as expected due to the silane overlayer. Figure 5d and the surface roughness value clearly show that APS assumes the glass surface morphology. This is an indication of a better wettability of glass with APS rather than with alkylsilanes. APS perhaps has a more favourable interaction with the glass substrate because of acid–base interactions between the basic -NH_2 pendent groups of APS and the acidic -SiOH silanol groups from the glass substrate surface.

Table 7 Average roughness (*Ra*) for untreated and organosilane-treated glass plates

Substrate	*Ra* (nm)
Glass	0.241
Glass–C1	6.583
Glass–C3	1.621
Glass–C8	5.164
Glass–APS	0.755

SEM characterization of PPy-coated glass substrates

SEM images of glass–PPy, glass–C1–PPy, glass–C3–PPy, glass–C8–PPy and glass–APS–PPy are shown in Fig. 6. On the micrometre scale, PPy deposition at the surface of untreated glass and glass–C1 led to the formation of wrinkled overlayers similar to those previously obtained by Pigois-Landureau et al. [29] at the surface of KOH-treated and chromic acid treated glass plates; however, the PPy overlayer appears smooth when coated on glass–C3, glass–C8 and glass–APS. On the latter substrate, the PPy coatings were much more continuous. In the present study, three wrinkles of length 30–60 μm join together to form domains, the centre of which is the starting point of each wrinkle. It is interesting to note that the surface of glass–PPy exhibits almost twice as many wrinkles as the surface of glass–C1–PPy. Pigois-Landureau et al. [29] interpreted the formation of wrinkles as a result of polymer shrinking on drying and also to an adhesion loss due to interfacial deprotonation of PPy. The continuous PPy films shown in Fig. 6c–e were obtained on the most hydrophobic surfaces (glass–C3, glass–C8 and glass-APS). This parallels the conclusions of Pigois-Landureau et al. [29] concerning the wrinkled morphology of PPy films on the hydrophilic KOH-treated glass surface in

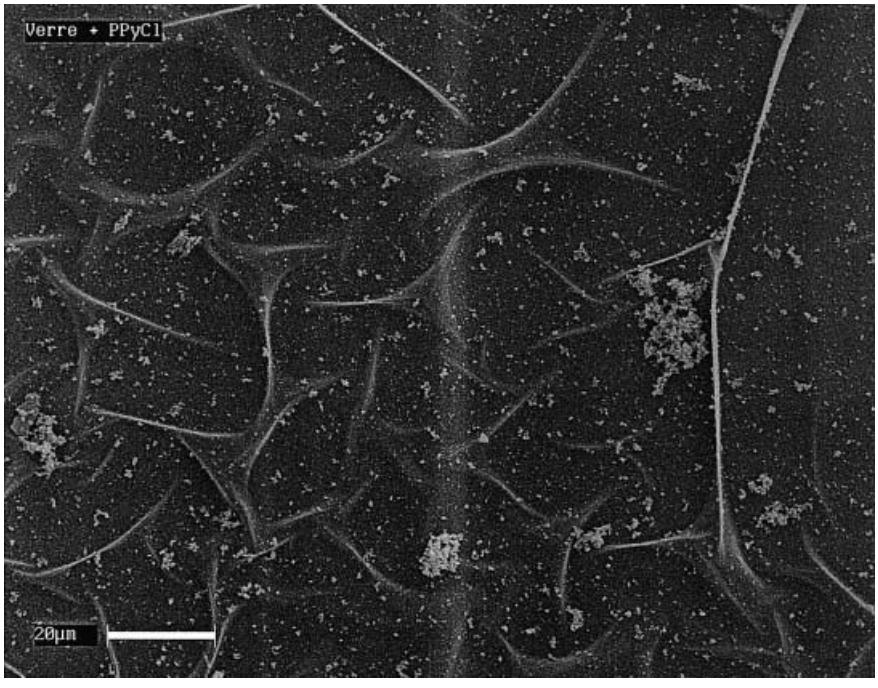

Fig. 6 Scanning electron microscope images of **a** glass–PPy, **b** glass–C1–PPy, **c** glass–C3–PPy, **d** glass–C8–PPy and **e** glass–APS–PPy

Fig. 6 (Contd.)

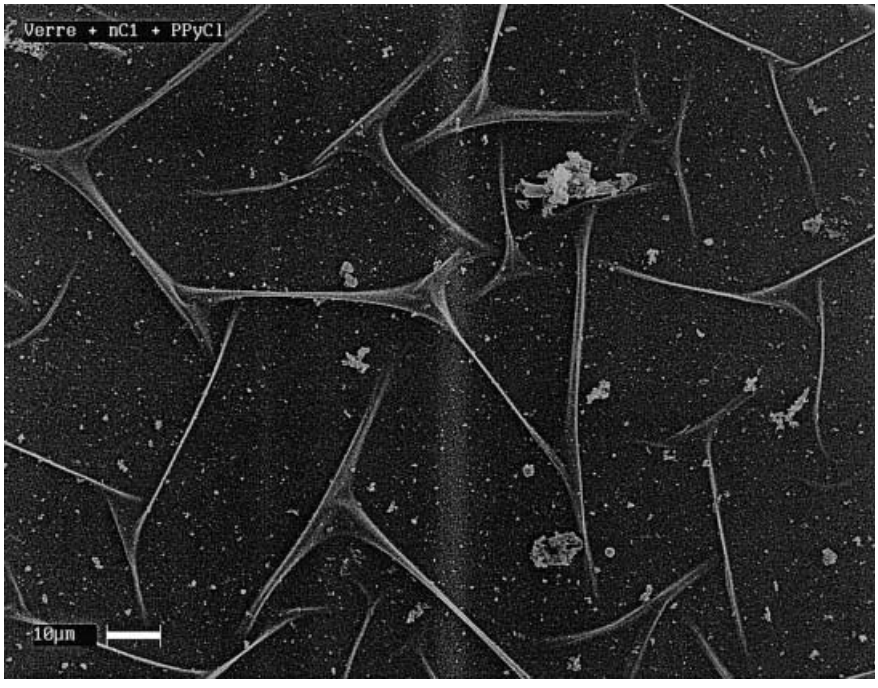

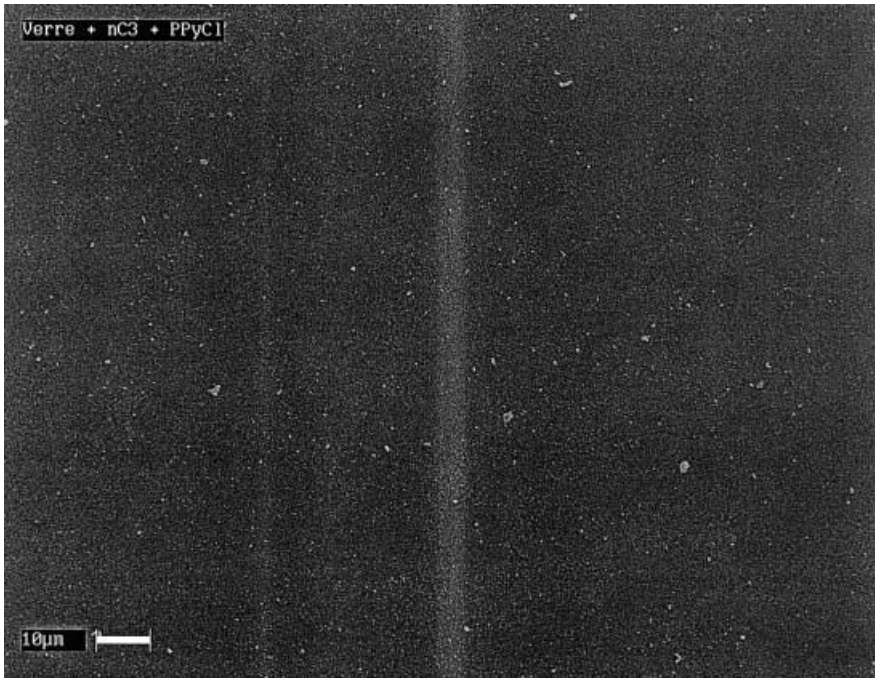

comparison to the more continuous films obtained on the hydrophobic chromic acid treated glass.

Adhesive tape peel test

Simple and qualitative adhesion tests were performed on the PPy-coated glass plates. Photographs of glass–C8–PPy and glass–APS–PPy after a 90° peel test are shown in Fig. 7. In Fig. 7a, it can be seen that most of the PPy overlayer has been removed by the adhesive tape (similar results were obtained for glass, glass–C1 and glass–C3 plates). This is in line with the findings of Huang et al. [15] that PPy can be removed from a C18-treated glass surface. In contrast, Fig. 7b shows that the adhesive tape remained stuck to the PPy coating, a qualitative

Fig. 6 (Contd.)

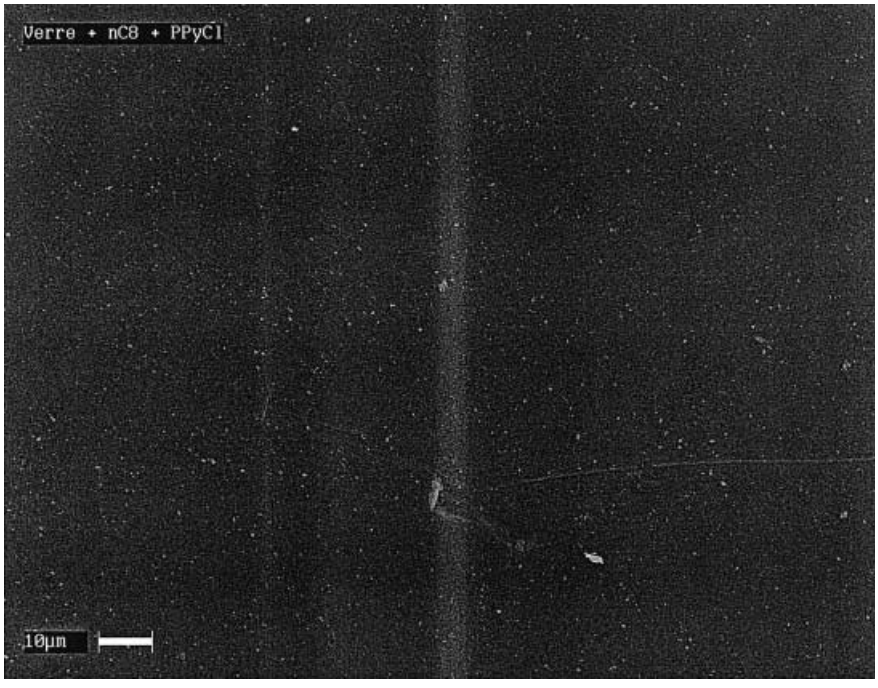

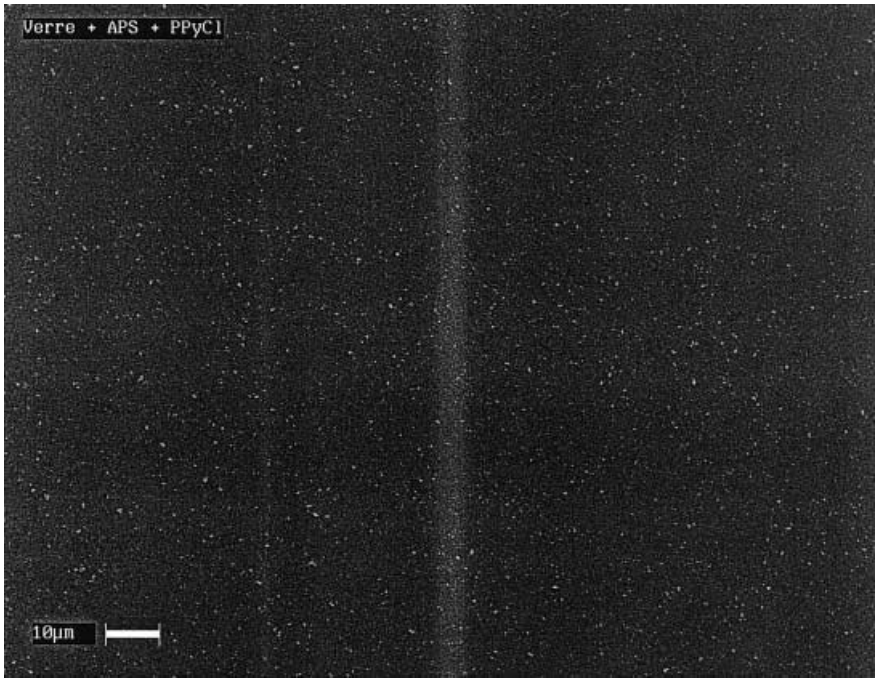

indication of stronger adhesion of PPy to the glass–APS than to the glass–C8 substrate.

Discussion

Surface treatment of glass substrates by a series of organosilanes was evidenced by both XPS and wettability water contact angle measurements. XPS shows elemental and chemical surface modification of glass by both the organosilanes and the PPy top layer. The surface chemical modification by the organosilanes led to a dramatic change in the hydrophilic/hydrophobic character of glass as measured by water contact angles. In the series of alkylsilanes, there is a close relationship between the number of carbon atoms in the coupling

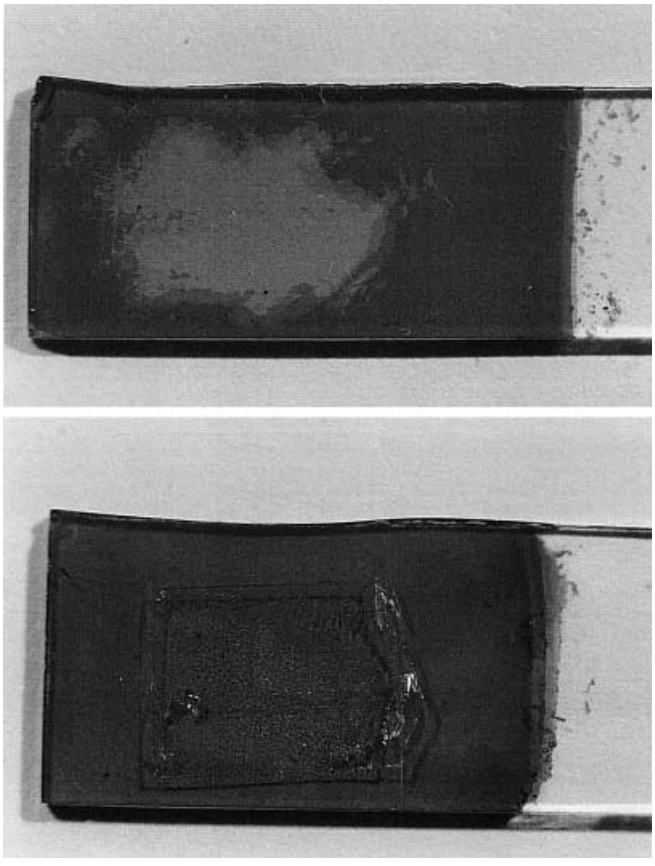

Fig. 7 Photographs of **a** glass–C8–PPy and **b** glass–APS–PPy following a 90° peel test using 3M double-sided adhesive tape

agent and the contact angle. It is interesting to note that APS and C8 led to similar wettability by water although these organosilanes differ significantly in size and nature, the former being Lewis basic in nature, whilst the latter is likely to interact only by dispersive interactions. AFM was found to be very effective in detecting the changes in the surface morphology of glass by grafting organosilanes. For comparable hydrophobic characters, glass–C8 and glass–APS have completely differing structures, resulting in a very low roughness of glass–APS (0.755 nm) compared to that of glass–C8 (5.164 nm). SEM did not show any significant difference between the morphology of PPy coatings at the surfaces of glass–C8 and glass–APS, and both PPy-coated plates appeared smooth. However, the peel test provides very useful qualitative information in that the adhesion of PPy to glass–APS is much stronger than the adhesion to glass–C8. This shows that the roughness effect, as observed by AFM, in the case of glass–C8 can be ruled out and adhesion by mechanical interlocking is thus not a key parameter for the adhesion of PPy to silanized glass.

PPy has a certain degree of hydrophobic character (contact angle of water is about 80° for tosylate-doped PPy) and is thus expected to interact with (untreated and organosilane-treated) glass by hydrophobic interactions. These interactions seem to be important in obtaining a good wetting of glass by PPy since a smooth overlayer is obtained in the case of glass–C3, glass–C8 and glass–APS but not in the case of glass and glass–C1. However, the peel test shows that strong practical adhesion was obtained in the case of glass–APS only; therefore, another parameter must govern PPy–glass adhesion. Since PPy is known to be an amphoteric polymer [23] whilst glass–APS has a basic character [30], the polymer and the substrate interact by acid–base interactions (or hydrogen bonding). Such interactions were evidenced by the peculiar structure of the N_{1s} peak for glass–APS–PPy. Therefore, acid–base interactions appear to be the driving force in promoting adhesion of PPy to glass, a situation that has been demonstrated for many polymer–substrate systems [31–32]. Acid–base interactions cannot, of course, occur at the PPy–alkylsilane interface since alkyl groups do not have acid–base properties.

To summarize, the hydrophobic character of the substrate is important for a good wetting of PPy and the formation of smooth overlayers, but acid–base interactions are essential for obtaining strong and durable adhesion.

Conclusion

PPy coatings were chemically synthesized at the surface of untreated, alklysilane-treated and aminosilane-treated glass plates. The glass, glass–silane and glass–silane–PPy plate surfaces were examined by water contact angle measurements, XPS, AFM and SEM. The adhesion of PPy to untreated and silanized-glass plates was checked by a peel test. Organosilane treatment clearly leads to an increase in the hydrophobic character of the glass substrate, depending on the nature and length of the silane pendant group. AFM indicated significant changes in the structure and roughness of the grafted organosilanes. XPS was effective in determining the surface composition of glass substrates before and after treatment by the silanes and/or coating with PPy. Moreover, the N_{1s} peak from glass–APS–PPy suggests that acid–base interactions occur between PPy and glass–APS. SEM shows that smooth PPy coatings were only obtained on the most hydrophobic surfaces, whereas wrinkled PPy coatings were observed at the relatively hydrophilic surfaces. Finally, a qualitative peel test showed that strong practical adhesion of PPy was obtained with the glass–APS substrate only. Our results show the role of organosilanes in promoting wettability of glass by conducting PPy. This wettability is likely to be driven by hydrophobic interactions. However, to achieve strong adhesion, acid–base interactions were found to be essential. Such interactions occurred only

between the predominantly Lewis acidic PPy and the Lewis basic amino group of APS. Since this interaction was evidenced by XPS, we suggest that the interaction of PPy with glass–APS results in the formation of an interphase rather than a sharp interface, a situation that is likely to occur in the case of alkylsilanes.

Acknowledgements C.P. is indebted to the French Ministry of Education and Research for financial support. We would like to thank the French Foreign Office, the Polish Academy of Science and the British Council for financial support through the Alliance (n°. 96092) and the Polonium (n°. 98053) schemes.

References

1. Naarman H (1991) Synth Met 1:41–43
2. Rodriguez J, Grande HJ, Otero TF (1997) In: Nalwa HS (ed) Handbook of organic conducting molecules and polymers, vol 2. Wiley, New York, p 415
3. Maeda S, Armes SP (1993) J Colloid Interface Sci 159:257
4. Maeda S, Armes SP (1994) J Mater Chem 4:935
5. Maeda S, Gill M, Armes SP, Fletcher IW (1995) Langmuir 11:1899
6. Butterworth MD, Corradi R, Johal J, Lascelles SF, Maeda S, Armes SP (1995) J Colloid Interface Sci 174:510
7. Goller MI, Barthet C, McCarthy GP, Corradi R, Newby BP, Wilson SA, Armes SP, Luk SY (1998) Colloid Polym Sci 276:1010
8. Faverolle F, Attias AJ, Bloch B, Audebert P, Andrieux CP (1998) Chem Mater 10:740
9. Chriswanto H, Ge H, Wallace GG (1993) Chromatographia 37:423
10. Ge H, Wallace GG (1991) J Chromatogr 588:25
11. Mittal KL (ed.) (1992) Silanes and other coupling agents. VSP, Utrecht
12. Gübitz G (1988) In: Frei RW, Zech K (eds) Selective sample handling and detection in high performance liquid chromatography. Journal of Chromatography Library, vol 39A, Elsevier, Amsterdam, pp 145–207
13. Miksa B, Slomkowski S, Chehimi MM, Delamar M, Majoral J-P, Caminade A-M (1999) Colloid Polym Sci 277:58
14. van Ooij WJ, Edwards RA, Sabata A, Zappia J (1993) J Adhes Sci Technol 7:897
15. Huang Z, Wang PC, MacDiarmid AG, Xia Y, Whitesides G (1997) Langmuir 13:6480
16. Perruchot C, Chehimi MM, Delamar M, Fievet F (1998) Surf Interface Anal 26:689
17. Perruchot C, Chehimi MM, Mordenti D, Briand M, Delamar M (1998) J Mater Chem 8:2185
18. Maeda S, Armes SP (1995) Synth Met 73:151
19. Wang D, Jones FR (1993) J Mater Sci 28:2481
20. Kowalczyk D, Slomkowski S, Chehimi MM, Delamar M (1996) Int J Adhes Adhesives 16:227
21. Kang ET, Neoh KG, Tan KL (1993) Adv Polym Sci 106:135
22. Sabbatini L, Malitesta C, De Giglio E, Losito I, Torsi L, Zambonin PG (1999) J Electron Spectrosc Relat Phenom 100:35
23. Chehimi MM, Abel M-L, Perruchot C, Delamar M, Lascelles SF, Armes SP (1999) Synth Met 104:51
24. Borade R, Sayari A, Adnot A, Kaliaguine S (1990) J Phys Chem 94:5989
25. Watts JF, Chehimi MM, Gibson EM (1992) J Adhes 39:145
26. Chehimi MM, Delamar M, Kurdi J, Arefi-Khonsari F, Lavaste V, Watts JF In: Mittal KL, Lacombe RH (eds) (in press) Acid–base interactions. Relevance to adhesion science and technology, vol 2. VSP, Utrecht
27. Seah MP, Dench WA (1979) Surf Interface Anal 1:2
28. Perruchot C, Chehimi MM, Delamar M, Lascelles SF, Armes SP (1996) Langmuir 12:3245
29. Pigois-Landureau E, Nicolau YF, Delamar M (1995) Synth Met 72:111
30. Tiburcio AC, Manson JA (1991) J Appl Polym Sci 42:427
31. Mittal KL, Anderson HR Jr (eds) (1991) Acid–base interactions. Relevance to adhesion science and technology. VSP, Utrecht
32. Mittal KL, Lacombe RH (eds) (in press) Acid–base interactions. Relevance to adhesion science and technology, vol 2. VSP, Utrecht